Environmental Science & Technology

Article

pubs.acs.org/est

Profiling the Serum Albumin Cys34 Adductome of Solid Fuel Users in Xuanwei and Fuyuan, China

Sixin S. Lu,[†] Hasmik Grigoryan,[¶,▽] William M. B. Edmands,[¶] Wei Hu,[§] Anthony T. Iavarone,[∥] Alan Hubbard,[‡] Nathaniel Rothman,[§] Roel Vermeulen,[⊥] Qing Lan,[§,▽] and Stephen M. Rappaport*[,¶,▽]

[†]Department of Nutritional Sciences and Toxicology, College of Natural Resources, University of California, Berkeley, California 94720, United States

[¶]Division of Environmental Health Sciences, School of Public Health, University of California, Berkeley, California 94720, United States

[§]Department of Health and Human Service, Division of Cancer Epidemiology and Genetics, National Cancer Institute, National Institutes of Health, Rockville, Maryland 20850, United States

[∥]California Institute for Quantitative Biosciences, University of California, Berkeley, California 94720, United States

[‡]Division of Biostatistics, School of Public Health, University of California, Berkeley, California 94720, United States

[⊥]Division of Environmental Epidemiology, Institute for Risk Assessment Sciences, Utrecht University, 3508 TD Utrecht, The Netherlands

Supporting Information

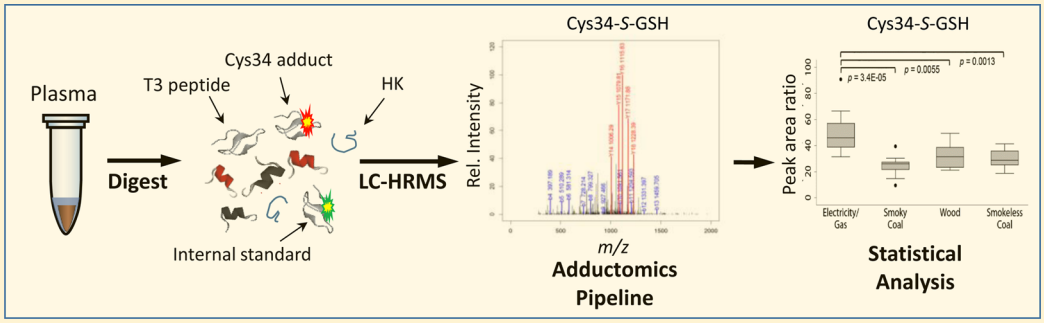

ABSTRACT: Xuanwei and Fuyuan counties in China have the highest lung cancer rates in the world due to household air pollution from combustion of smoky coal for cooking and heating. To discover potential biomarkers of indoor combustion products, we profiled adducts at the Cys34 locus of human serum albumin (HSA) in 29 nonsmoking Xuanwei and Fuyuan females who used smoky coal, smokeless coal, or wood and 10 local controls who used electricity or gas fuel. Our untargeted "adductomics" method detected 50 tryptic peptides of HSA, containing Cys34 and prominent post-translational modifications. Putative adducts included Cys34 oxidation products, mixed disulfides, rearrangements, and truncations. The most significant differences in adduct levels across fuel types were observed for *S*-glutathione (*S*-GSH) and *S*-γ-glutamylcysteine (*S*-γ-GluCys), both of which were present at lower levels in subjects exposed to combustion products than in controls. After adjustment for age and personal measurements of airborne benzo(*a*)pyrene, the largest reductions in levels of *S*-GSH and *S*-γ-GluCys relative to controls were observed for users of smoky coal, compared to users of smokeless coal and wood. These results point to possible depletion of GSH, an essential antioxidant, and its precursor γ-GluCys in nonsmoking females exposed to indoor-combustion products in Xuanwei and Fuyuan, China.

INTRODUCTION

Lung cancer is the leading cause of cancer mortality worldwide.[1] While most lung cancers can be attributed to cigarette smoking, in East Asia an estimated 61% of female lung cancers are observed in never-smokers,[2] especially those exposed to household air pollution from coal combustion.[3] Domestic fuel combustion has been recognized as a major source of exposure to carcinogens that affects about 3 billion people worldwide.[4] Indeed, Xuanwei and Fuyuan Counties in China, where smoky (bituminous) coal is used for domestic cooking and heating, have the highest lung cancer incidence and mortality in the world.[5,6]

Since women from Xuanwei and Fuyuan rarely smoke, the high incidence of lung cancer has motivated scrutiny of possible risk factors. Nonsmoking Xuanwei women, who use smoky coal, have a 30-fold greater risk of lung cancer than those who use smokeless (anthracite) coal or wood.[7] Compared to smokeless coal, smoky coal emits significantly more particulate matter (PM),

Received: August 17, 2016
Revised: November 16, 2016
Accepted: November 18, 2016
Published: November 18, 2016

DOI: 10.1021/acs.est.6b03955
Environ. Sci. Technol. 2017, 51, 46−57

polycyclic aromatic hydrocarbons (PAHs), and silica, all of which are known lung carcinogens.[6,8−10] Of these potentially causal exposures in Xuanwei, PAHs have been scrutinized, on the basis of the detection of PAH−DNA adducts,[11] characteristic mutational spectra in lung tumors,[12] and risk modulation by genes involved in PAH metabolism.[13,14] However, the heterogeneity of emissions of PAHs and other combustion products, even across subtypes of smoky coal, has complicated the analysis of exposure−response relationships.[7−10]

Many environmental toxicants that emanate from combustion of solid fuels either are reactive electrophiles or are metabolized to such species in the body. Reactive electrophiles can produce DNA mutations and modify functional proteins[15,16] and can alter the redox proteome.[17] Since reactive electrophiles have short lifetimes, investigators have studied their dispositions in vivo by measuring adducts from reactions with abundant proteins in the blood, mainly hemoglobin and human serum albumin (HSA).[18] HSA is particularly interesting because it contains a nucleophilic hotspot, Cys34, that efficiently scavenges reactive oxygen species (ROS) and other small electrophiles in serum, where it represents about 80% of the antioxidant capacity.[19] Oxidation of Cys34 to the reactive sulfenic acid (Cys34-SOH) can lead to formation of mixed Cys34-disulfides from reactions between Cys34-SOH and circulating low-molecular-weight thiols.[20] These Cys34 disulfides represent potential biomarkers of the redox state of the serum over the 1 month residence time of HSA.[21,22]

Our laboratory has recently developed an *untargeted* assay for characterizing modifications at the Cys34 locus of HSA that we refer to as "Cys34 adductomics".[23] The scheme focuses on the third largest tryptic peptide of HSA ("T3") with a sequence of ALVLIAFAQYLQQC[34]PFEDHVK and a mass of 2432 Da. Adducts of this hydrophobic peptide are separated by nanoflow liquid chromatography (nLC) and detected by high-resolution mass spectrometry (HRMS). A bioinformatic pipeline is used to locate T3 modifications from tandem MS2 spectra, to annotate modifications based on accurate masses, and to quantitate and normalize peak areas.

Given the constellation of electrophiles generated during combustion of fossil fuels, it is difficult to hypothesize about particular adducts or classes of protein modifications that might be observed in blood from Xuanwei and Fuyuan subjects. Cys34 adductomics offers a data-driven approach for comparing adduct features across populations differentially exposed to combustion effluents and thereby for discovering potential biomarkers of relevance to human health. Discriminating adduct features can be identified and targeted for follow-up studies to investigate effects of exposure and to develop mechanistic understanding. Here, we describe application of our methodology to characterize Cys34 adducts in plasma from 29 healthy nonsmoking women from Xuanwei and Fuyuan, China, who used smoky coal, smokeless coal, or wood and 10 local controls who used electricity/gas. We detected 50 T3-derived peptides in these women and explored relationships between adduct levels and the types of solid fuel as well as personal measurements of airborne PM and a carcinogenic PAH (benzo(*a*)pyrene, BaP). Despite the small sample sizes, we detected several highly significant associations between adduct levels and covariates that should generate hypotheses for follow-up studies.

EXPERIMENTAL SECTION

Reagents. Acetonitrile (LC/MS grade), dimethyl sulfoxide, ethylenediaminetetraacetic acid, triethylammonium bicarbonate buffer (1 M), and trypsin (from porcine pancreas, catalog number T0303) were from Sigma-Aldrich (St. Louis, MO). Formic acid and methanol were from Fisher Scientific (Optima LC/MS, Fair Lawn, NJ). Water (18.2 mΩ cm resistivity at 25 °C) was purified by a PureLab Classic system (ELGA LabWater, Woodridge, IL). Isotopically labeled T3 peptide (iT3) with sequence AL-[^{15}N,^{13}C-Val]-LIAFAQYLQQCPFEDH-[^{15}N,^{13}C-Val]-K was custom-made (>95%, BioMer Technology, Pleasanton, CA). The carbamidomethylated iT3 peptide (IAA-iT3) was used as an internal standard for monitoring mass and retention time (RT) stabilities and was prepared as reported previously.[24]

Plasma Samples and Air Measurements. Plasma samples were obtained with informed consent from subjects in China under protocols approved by the National Cancer Institute and local Chinese institutions. Plasma from 29 nonsmoking female subjects using smoky coal, smokeless coal, or wood (hereafter, "exposed subjects") was collected in 2008 and 2009 as part of a cross sectional study in Xuanwei and Fuyuan counties, China. Details of this study, including the demographic characteristics of the subjects, and collection of air and biological samples have been described.[8−10,25,26] Blinded duplicate aliquots from four exposed subjects were also included to assess sample-processing variability and quality assurance, resulting in a total of 33 plasma samples from exposed subjects. Archived plasma from 10 nonsmoking female electricity or gas users (hereafter, "control subjects") were collected between 2007 and 2010 in nearby hospitals in Fuyuan, Qujing, and Xuanwei Counties. Control subjects were being treated for conditions unrelated to tobacco smoking, smoky coal use, and lung disease and had the same age distribution as the exposed subjects. Plasma samples were stored at −80 °C for 4−8 years before analysis.

Personal $PM_{2.5}$ samples (i.e., PM with aerodynamic diameter less than 2.5 μm) were collected on Teflon filters for all exposed subjects in the 24 h period prior to the blood draw.[8,9] Nineteen of these samples were extracted with dichloromethane and analyzed for BaP by gas chromatography−mass spectrometry.[9] Exposed subjects, for whom BaP exposures were not measured, were imputed the median BaP levels estimated among other subjects with the same type of fuel. Three categories of BaP and $PM_{2.5}$ exposures were established as follows: controls, low exposure (below the median value), or high exposure (at or above the median value) (median values: BaP = 36.7 ng/m^3, $PM_{2.5}$ = 145 μg/m^3). Personal BaP and $PM_{2.5}$ levels for the 10 control subjects were imputed the minimum values observed in any exposed subject divided by $\sqrt{2}$. Table S1 provides summary statistics for selected variables (age, BMI, and concentrations of BaP and PM2.5) across the 39 subjects stratified by fuel type.

Sample Processing. The 43 plasma samples were processed in four random batches of 10 or 11 samples. Samples were analyzed as previously described.[23] Briefly, 5 μL of plasma was mixed with 60 μL of 50% methanol for 15 min and centrifuged. Fifty microliters of the supernatant was mixed with 200 μL of digestion buffer (50 mM triethylammonium bicarbonate, 1 mM ethylenediaminetetraacetic acid, pH 8.0) and stored at −80 °C prior to digestion. One hundred thirty-eight microliters of the solution was transferred to a MicroTube (MT-96, Pressure Biosciences Inc., South Easton, MA) to which 2 μL of 10 μg/μL trypsin was added (~1:10 ratio of trypsin/protein, w/w). The tube was capped (MC150-96, Pressure Biosciences Inc.), vortexed briefly, and placed in a pressurized system (Barocycler NEP2320, Pressure Biosciences Inc.) that cycled between 1380 bar (45 s) and ambient pressure

DOI: 10.1021/acs.est.6b03955
Environ. Sci. Technol. 2017, 51, 46−57

(15 s) for 30 min at 37 °C. We had previously shown that pressure cycling of serum/plasma extracts containing 10−20% methanol promoted rapid tryptic digestion, even without prior reduction of disulfide bonds in HSA.[23] After digestion, 3 μL of 10% formic acid was added to stop digestion, and the digest was briefly vortexed and centrifuged to remove particles. Twenty microliters of the digest and 1 μL of a 20 pmol/μL solution of internal standard (IAA-iT3) were transferred to a silanized autosampler vial containing 79 μL of an aqueous solution of 2% acetonitrile and 0.1% formic acid. The diluted digest was stored at −80 °C and/or queued at 4 °C for up to 36 h prior to analysis by nLC-HRMS.

Nanoflow Liquid Chromatography−Mass Spectrometry. Digests were analyzed by nLC-HRMS with an LTQ Orbitrap XL Hybrid mass spectrometer coupled to a Dionex UltiMate 3000 nLC system via a Flex Ion nanoelectrospray ionization source (Thermo Fisher Scientific, Waltham, MA), operated in positive ion mode, as described previously.[23] Briefly, duplicate 1 μL portions of each diluted digest were injected into the nLC and separated on a Dionex PepSwift monolithic column (100 μm i.d. × 25 cm) (Thermo Scientific, Sunnyvale, CA, USA). Full scan MS spectra (m/z 350−1200) were acquired with a resolution of 60 000 at m/z 400 in the Orbitrap. In data-dependent mode, up to six intense triply charged precursor ions from each MS1 scan were fragmented by collision-induced dissociation and tandem mass spectra (MS2) were acquired in the linear ion trap. The column was washed after every pair of duplicate injections with 1 μL of a solution containing 80% acetonitrile, 10% acetic acid, 5% dimethyl sulfoxide, and 5% water.

Locating T3-Related Peptides with MS2 Spectra. As described previously,[23] RAW data files were converted to mzXML format using the ProteoWizard msConvert tool (3.06387, 64-bit)[27] without filters. All MS2 spectra collected in the elution window between 20 and 35 min were screened for putative adducts using in-house software written in R.[28] Briefly, the screening algorithm focused on signature ions from the T3 peptide and required the presence of at least five unmodified b^+-series fragment ions with signal-to-noise ratios >3 (b_3^+−b_6^+ and b_{11}^+−b_{13}^+) plus a set of at least four fragment ions indicative of the prominent y_{14}^{2+} through y_{18}^{2+} ions with relative intensities ≥20% of the base peak. Spectra that passed the screening algorithm were considered to represent T3-related peptides. These T3 peptides were then clustered with each nearest neighbor having a monoisotopic mass (MIM) within 0.003 m/z and a RT within 0.4 min. For each group, an isotope distribution consistent with its respective triply charged precursor MIM was verified, and the means of MIMs and RTs were calculated. Representative MS2 spectra of all putative T3 adducts are shown in Figure S1.

Annotation of Putative Adducts. Putative T3 adducts were annotated as described previously.[23] Briefly, the masses added to the thiolate form of the T3 peptide (Cys34-S^-) were calculated and plausible elemental compositions were probed or confirmed using ChemCalc Molecular Formula finder,[29] Molecular Weight Calculator (version 6.50, https://omics.pnl.gov/software/molecular-weight-calculator/), UNIMOD (http://www.unimod.org/), and MetFrag.[30] Mass accuracy of the assigned elemental composition was assessed in terms of the difference (<3 ppm) between theoretical and observed MIMs. A modification at Cys34 is indicated by MS2 spectra displaying unmodified y_7^+ or y_7^{2+} (i.e., from Pro35 to the C-terminus) plus mass-shifted b_{14}^+ (i.e., from the N-terminus to Cys34), y_8^+, or y_8^{2+} (i.e., from Cys34 to the C-terminus). Conversely, the presence of unmodified b_{14}^+, y_8^+, and y_8^{2+} indicates that modification(s) were not at Cys34.[23] Adducts lacking unambiguous diagnostic ions were annotated as having unclear modification sites. Evidence for annotations is given in Table S2.

Quantitation of T3-Related Peptides. Automated peak integration of T3-related peptides was performed using Processing Methods in Xcalibur software (version 2.0.7 SP1, Thermo Fisher Scientific, Inc., Waltham, MA) based on MIMs and RTs with 5 ppm mass accuracy using the Genesis algorithm without smoothing and with >3 signal-to-noise ratio. Each low-abundance peak of a putative T3 peptide was verified by comparing the observed isotopic pattern against the expected pattern. To quantitate and adjust adduct levels for the amounts of HSA in individual digests, peak areas were divided by the corresponding peak areas of a "housekeeping peptide" (HK), with sequence LVNEVTEFA, that appears as a doubly charged peptide (MIM = 575.31113 m/z; average RT = 13.5 min). The peak area ratio (PAR, adduct peak area/HK peak area) was previously shown to be a robust linear predictor of adduct concentrations over at least a 500-fold range (0.01−5 μM).[23] Approximate adduct concentrations with units of pmol adduct/mg HSA were estimated as previously described.[23]

Batch Adjustment. Peak-area ratios were log-transformed and adjusted for batch effects with a mixed-effects model similar to that described previously,[23] using Stata software (Stata Statistical Software: Release 13. College Station, TX). Since data included four blinded sample replicates as well as injection replicates for all samples, the following model was used:

$$\ln\left(\frac{\text{adduct}}{\text{HK peptide}}\right) = \beta_0 + \beta_{1_i} + \mu_{0_j} + \mu_{1_{jk}} + \varepsilon_{ijkh} \quad (1)$$

where β_0 is the fixed overall mean value of the logged peak-area ratio (intercept), β_{1_i} is the fixed effect for the i^{th} batch, μ_{0_j} is the random effect for the j^{th} subject, $\mu_{1_{jk}}$ is the random effect for the k^{th} replicate sample from the j^{th} subject (duplicate samples from four subjects), and ε_{ijkh} is the residual error for the h^{th} injection for a given sample (duplicate injections for all subjects). Restricted maximum likelihood (REML) estimation was used to fit the models. Coefficients of variation (CVs), representing sample replicates and duplicate injections, were estimated as $\sqrt{e^{(\widehat{\sigma}_P{}^2-1)}}$ or $\sqrt{e^{(\widehat{\sigma}_M{}^2-1)}}$, respectively, where $\widehat{\sigma}_P{}^2$ is the estimated variance component for replicate samples and $\widehat{\sigma}_M{}^2$ is the estimated variance component for replicate injections. Intraclass correlation coefficients (ICCs) were estimated as $\text{ICC} = \frac{\widehat{\sigma}_B{}^2}{\widehat{\sigma}_B{}^2 + \widehat{\sigma}_P{}^2 + \widehat{\sigma}_M{}^2}$, where $\widehat{\sigma}_B{}^2$ is the estimated between-subject variance component. Adducts whose models failed to fit (n = 2) or with ICCs < 0.1 (n = 12) were eliminated from statistical testing; however, each of their median levels was estimated across subjects with PARs.

After batch adjustment with model (1), subject-specific PARs were predicted as $\ln(\text{PAR}) = \beta_0 + \mu_{0_j}$ for each adduct[23] and these values were used for statistical tests. When a given adduct was not detected in all replicates from a given subject, the ln(PAR) was imputed a value of $minimum - \ln(\sqrt{2})$ where $minimum$ is the smallest ln(PAR) of a given adduct observed in any subject. Among 36 adducts with ICCs ≥ 0.1, 11 had between 1 and 39 nondetected values (median = 15).

Four sets of structurally related adducts were collapsed into clusters, namely, two peaks of S-homocysteine (S-hCys), and

DOI: 10.1021/acs.est.6b03955
Environ. Sci. Technol. 2017, 51, 46−57

Table 1. Putative T3 Peptides in the Current Study

adduct	retention time (min)	PAR[a] (×10 000)	concn[b] (pmol/mg HSA)	*m/z*, 3+, observed	mass (Da) added to T3 (Cys-S$^-$)	added mass composition	*m/z*, 3+, theoretical	Δmass (ppm)	putative annotation
M1	27.79	4.56	2.00	796.43091	−45.98870	$-CH_2S$	796.43009	−1.03	Cys34 → Gly
M2	28.83	0.476	0.208	800.43213	−33.98505	$-H_2S$	800.43009	−2.54	Cys34 → dehydroalanine
M3	27.40	2.33	1.02	805.76263	−17.99356	$-H_2S$, +O	805.76173	−1.11	Cys34 → oxoalanine
M4	27.95	0.781	0.341	808.73005	−9.09130				not Cys34 adduct
M5	27.88	26.7	11.7	811.76011	1.0072		811.75933	−0.95	T3 labile adduct
M6	28.49	399	174	811.76048	1.00831		811.75933	−1.41	unadducted T3[d]
M7	30.35	26.5[c]	11.6	811.42514	2431.24780	$+C_{114}H_{172}N_{27}O_{30}S$	811.42394	−1.47	T3 dimer[d]
M8	27.30	19.5	8.53	816.42006	13.97875	$-H_2$, +O	816.41909	−1.19	Cys34-Gln cross-link[d]
M9	28.92	5.53	2.42	816.43203	15.02192	$+CH_3$	816.43122	−0.99	methylation, not Cys34
M10	28.51	2.69	1.18	819.08685	22.98639	M6−H + Na	819.08665	−0.24	Na adduct of M6
M11	27.30	30.4	13.3	822.42354	32.99646	$+HO_2$	822.42261	−1.13	sulfinic acid[d]
M12	28.51	1.47	0.644	824.41032	38.95681	M6−H + K	824.41130	1.18	K adduct of M6
M13	29.51	1.28	0.558	827.09009	46.99610	$+CH_3S$	827.08858	−1.83	*S*-methylthiolation
M14	27.63	4.54	1.99	827.75482	48.99030	$+HO_3$	827.75425	−0.69	sulfonic acid[d]
M15	28.50	1.43	0.624	829.39659	53.91560				unclear modification site
M16	27.40	4.38	1.91	841.09883	89.02234	$+C_3H_5O_3$	841.09802	−0.97	pyruvate or malonate semialdehyde
M17	28.25	7.35	3.21	841.75250	90.98332	$+C_2H_3O_2S$	841.75185	−0.76	*S*-mercaptoacetic acid
M18	27.27	14.9	6.52	845.42505	102.00098	$+C_3H_4NOS$	845.42385	−1.42	*S*-Cys ($-H_2O$)
M19	28.55	0.457	0.200	845.75278	102.98417	$+C_3H_3O_2S$	845.75185	−1.09	*S*-Cys (possibly NH_2 → OH, $-H_2O$)
M20	29.53	1.98	0.867	847.10752	107.04839	$+C_7H_7O$	847.10662	−1.06	benzaldehyde
M21	27.29	0.497	0.217	847.76593	109.02363				Cys34 adduct with unknown annotation
M22	28.31	0.454	0.199	849.06903	112.93293	$+HO_3S_2$	849.06896	−0.08	*S*-*S*-sulfonic acid trisulfide
M23	28.12	1.28	0.559	850.09692	116.01661	$+C_4H_6NOS$	850.09573	−1.41	*S*-hCys ($-H_2O$)
M24	26.36	3640	1590	851.42850	120.01134	$+C_3H_6NO_2S$	851.42737	−1.33	*S*-Cys[d]
M25	27.70	15.1	6.60	851.75712	120.99719	$+C_3H_5O_3S$	851.75537	−2.05	*S*-Cys (NH_2 → OH)
M26	27.58	1.72	0.753	853.78324	127.07557				Cys34 adduct with unknown annotation
M27	29.02	0.186	0.0815	855.43732	132.03779	$+C_8H_6NO$	855.43837	1.23	oxindole
M28	26.61	170	74.3	856.10012	134.02621	$+C_4H_8NO_2S$	856.09925	−1.02	*S*-hCys[d]
M29	26.95	104	45.3	856.09983	134.02533	$+C_4H_8NO_2S$	856.09925	−0.68	*S*-hCys[d]
M30	27.70	7.56	3.31	857.09973	137.02503	$+C_4H_9O_3S$	857.09914	−0.69	Cys34 adduct with unknown annotation
M31	26.39	30.9	13.5	858.75401	141.98788	M24−H + Na	858.75468	0.78	Na adduct of M24
M32	27.06	3.30	1.44	860.77178	148.04118	$+C_5H_{10}NO_2S$	860.77113	−0.75	*S*-hCys, plus methylation not at Cys34
M33	26.38	33.6	14.7	864.07707	157.95704	M24−H + K	864.07933	2.62	K adduct of M24
M34	27.05	1.85	0.811	864.43189	159.02152	$+C_5H_7N_2O_2S$	864.43100	−1.03	*S*-CysGly ($-H_2O$)
M35	27.53	1.04	0.457	865.43150	162.02033	$+C_5H_8NO_3S$	865.43089	−0.70	*S*-(*N*-acetyl)Cys
M36	27.01	1.45	0.634	866.75716	165.99731	$+C_4H_8NO_2S_2$	866.75661	−0.63	*S*-*S*-hCys trisulfide
M37	26.10	316	138	870.43565	177.03279	$+C_5H_9N_2O_3S$	870.43452	−1.30	*S*-CysGly[d]
M38	26.32	4.58	2.00	875.10623	191.04454	M37 + CH_2	875.10640	0.20	*S*-CysGly, plus methylation not at Cys34
M39	27.66	1.18	0.516	875.42305	191.99498				Cys34 adduct with unknown annotation
M40	26.10	3.12	1.37	877.76149	199.01031	M37−H + Na	877.76184	0.40	Na adduct of M37
M41	26.14	3.55	1.55	883.08462	214.97971	M37−H + K	883.08648	2.11	K adduct of M37
M42	24.99	1.37	0.600	894.12694	248.10667				Cys34 adduct with unknown annotation
M43	26.67	22.6	9.89	894.44219	249.05241	$+C_8H_{13}N_2O_5S$	894.44156	−0.70	*S*-γ-GluCys
M44	26.55	31.6	13.8	913.44928	306.07367	$+C_{10}H_{16}N_3O_6S$	913.44872	−0.61	*S*-GSH[d]
M45	25.37	5.00	2.19	931.82122	361.18949				Cys34 adduct with unknown annotation
M46	25.30	1.03	0.450	941.15696	389.19672				unclear modification site
M47	25.40	22.9	10.0	965.49160	462.20064	$+C_{18}H_{32}N_5O_7S$	965.49080	−0.83	Cys34 adduct with unknown annotation
M48	25.33	1.92	0.840	974.50721	489.24747				Cys34 adduct with unknown annotation
M49	26.96	2.82	1.23	976.82030	496.18675				Cys34 adduct with unknown annotation

DOI: 10.1021/acs.est.6b03955
Environ. Sci. Technol. 2017, 51, 46−57

Table 1. continued

adduct	retention time (min)	PAR[a] (×10 000)	concn[b] (pmol/mg HSA)	m/z, 3+, observed	mass (Da) added to T3 (Cys-S⁻)	added mass composition	m/z, 3+, theoretical	Δmass (ppm)	putative annotation
M50	25.25	1.58	0.692	981.49559	510.21261				Cys34 adduct with unknown annotation

[a]Median peak-area ratio (adduct/housekeeping peptide) in natural scale before imputing nondetects. [b]Approximate adduct concentration. [c]6+ charge state, peak areas obtained by extracting the second heavy isotope ion (m/z 811.76, more readily detected than MIM). [d]Annotation confirmed with synthetic standard.

the respective sodium and/or potassium adducts of unadducted T3, *S*-cysteine (*S*-Cys), and *S*-cysteinylglycine (*S*-CysGly). For each cluster, predicted subject-specific logged adduct levels were exponentiated, summed, and log-transformed. After clustering, 32 adducts and clusters were subjected to statistical analyses.

Statistical Analyses. Statistical analyses were performed with Stata software using predicted logged PARs from model [1] (×10 000 for scaling) for each of the 32 adducts and clusters. Three permutation Kruskal–Wallis tests were performed using the *permute* command of Stata with 100 000 replications, under the null hypotheses that fuel types, BaP categories, or $PM_{2.5}$ categories had the same median adduct levels. Significance levels were corrected for multiple testing at a 5% uncorrected false discovery rate (FDR) using the *simes* option (Benjamini-Hochberg method)[31] of the *multproc* program.[32] For each significant Kruskal–Wallis test, a Wilcoxon rank sum test was performed between all pairs of exposure categories with the *dunntest* package[33] with significance levels corrected at 5% FDR using the *simes* option. Adducts with absolute values of Spearman correlation coefficients (r_S) greater than 0.5 were organized into a network generated with Cytoscape.[34] Multivariable linear regression was used to model each adduct or cluster as a function of the fuel types (as dichotomous variables) plus age and log-transformed levels of BaP as covariates. Exploratory analyses, using backward stepwise elimination, revealed that BMI and $PM_{2.5}$ were weaker predictors than fuel groups, BaP, and age and thus were not included in the multivariable models for power considerations.

RESULTS

Annotation of Adducts. The adductomics workflow identified 50 distinct T3-related peptides (numbered M1 through M50) as summarized in Table 1. Median adduct levels spanned a 19 500-fold range with PARs ranging from 0.19 to 3640, corresponding to approximate adduct concentrations of 0.080 to 1590 pmol/mg HSA. For 40 of the T3 peptides, the observed MIM was within 3 ppm of the theoretical value of a modification having a plausible elemental composition. Previously reported modifications[23] include truncations (M1–M4), a labile adduct (M5), unmodified T3 (M6), the T3 dimer (M7, 6+ charge state), T3 methylation at a site other than Cys34 (M9), and Cys34 oxidation products (M8, M11, and M14). The largest class of modifications consisted of 22 mixed disulfides of Cys34, most of which have been reported,[23] including two isomeric modifications of *S*-hCys (M28 and M29), four Na and K adducts of *S*-Cys and *S*-CysGly (M31, M33, M40, and M41), and two apparent modifications of *S*-hCys or *S*-CysGly (M32 and M38). Other putative adducts that have not been reported previously include: *S*-methylthiolation (M13), a Cys34 adduct of pyruvate or malonate semialdehyde (M16), a variant of the *S*-Cys adduct (M19, possibly $NH_2 \rightarrow OH$, $-H_2O$), a Cys34 adduct of oxindole (M27), and a Cys34 trisulfide, i.e. *S*-*S*-hCys (M36). Evidence used for annotation of all T3-related peptides is summarized in Table S2.

Summary Statistics and Global Comparisons. Median PARs (×10 000) and CVs are shown in Table 2 for all adducts or clusters. The levels of Cys34 oxidation products for a given subject always followed the order: sulfinic acid (dioxidation, M11) > Cys34-Gln cross-link (mono-oxidation, M8) ≫ sulfonic acid (trioxidation, M14), as previously reported for healthy volunteers.[23] Among 36 adducts with ICCs ≥ 0.1 (ICC: median = 0.73; range: 0.19–0.98), CVs for replicate injections (CV_M: median = 21%; range: 7.7–70%) tended to be greater than those for replicate samples (CV_P: median = 5.5%; range: 0–78%).

Table 2 also shows median adduct levels aggregated by fuel type and categories of BaP and $PM_{2.5}$ exposures, along with results of Kruskal–Wallis tests that investigated global associations for 32 adducts. After multiple testing correction (α = 0.0078), five adducts had significant differences across fuel groups, i.e., the T3 labile adduct (M5), the *S*-hCys cluster (M28 + M29), a Cys34 adduct with unknown annotation (M30, likely composition: $+C_4H_9O_3S$), *S*-γ-glutamylcysteine (*S*-γ-GluCys, M43), and *S*-glutathione (*S*-GSH, M44). The latter three adducts (M30, M43, and M44) also differed significantly across categories of exposures to both BaP and $PM_{2.5}$ (α = 0.0047).

Pairwise Differences between Exposure Categories. The sources of global differences across exposure categories (Table 2) were investigated pairwise with Wilcoxon rank sum tests, several of which had *P*-values that remained significant after corrections for multiple testing. Subjects using electric/gas fuel or smoky coal had significantly lower levels of the T3 labile adduct (M5) than those using wood or smokeless coal (Figure 1A); those using electric/gas fuel or smoky coal had significantly lower levels of *S*-hCys (M28 + M29) than those using smokeless coal, while those using electric/gas fuel also had significantly lower levels of *S*-hCys than those using wood (Figure 1B); those using either type of coal had significantly lower levels of *S*-γ-GluCys (M43) and *S*-GSH (M44) than those using electric/gas fuel (Figure 1D), and those using each solid fuel had significantly lower levels of a Cys34 adduct with unknown annotation (M30) and *S*-GSH (M44) than those using electric/gas fuel (Figure 1C,E).

Extending pairwise comparisons to subjects classified by exposures to BaP and $PM_{2.5}$, the global differences observed in Table 2 for a Cys34 adduct with unknown annotation (M30), *S*-γ-GluCys (M43), and *S*-GSH (M44) reflect significantly higher adduct levels in controls compared to either low- or high-exposed subjects for both BaP and $PM_{2.5}$ (Figure S2).

Correlation of Adduct Levels. Figure 2 shows a correlation map of the 25 adducts having at least one $|r_S|$ greater than 0.5 with another adduct. Many of the moderate to strong correlations were between structurally or biochemically related adducts. For example, *S*-GSH (M44) was correlated with *S*-γ-GluCys (M43), which in turn was correlated with *S*-Cys (M24). Unadducted T3 (M6) and the earlier-eluting *S*-hCys disulfide (M28) were strongly correlated with their methylated counterparts (M9 and M32, respectively). Unadducted T3 (M6),

DOI: 10.1021/acs.est.6b03955
Environ. Sci. Technol. 2017, 51, 46–57

Table 2. Median Peak-Area Ratios (adduct/HK × 10 000) in Natural Scale[a]

				medians for fuel type					medians for BaP exposure category				medians for $PM_{2.5}$ exposure category			
adduct or cluster	CV_P (%)	CV_M (%)	global median (n = 39)	control (n = 10)	smoky (n = 10)	wood (n = 9)	smokeless (n = 10)	KW P-value (95% CI)	control (n = 10)	low (n = 15)	high (n = 14)	KW P-value (95% CI)	control (n = 10)	low (n = 15)	high (n = 14)	KW P-value (95% CI)
M1	0	14.7	4.70	4.66	4.78	5.23	4.33	0.54 (0.54, 0.54)	4.66	4.30	5.04	0.23 (0.23, 0.23)	4.66	4.65	4.92	0.54 (0.54, 0.54)
M2	3×10^{-5}	40.2	0.431	0.441	0.478	0.397	0.438	n/a[c]	0.441	0.420	0.499	n/a[c]	0.441	0.420	0.449	n/a[c]
M3	0	25.7	2.40	2.86	2.37	2.65	2.16	0.29 (0.29, 0.29)	2.86	2.05	2.62	0.043 (0.042, 0.045)	2.86	2.42	2.20	0.29 (0.29, 0.29)
M4	28.4	33.6	0.784	1.38	0.678	0.635	0.789	0.035 (0.034, 0.036)	1.38	0.784	0.631	0.018 (0.017, 0.018)	1.38	0.635	0.748	0.035 (0.034, 0.036)
M5	12.6	16.4	28.9	24.9	21.7	32.5	33.4	**1.1×10^{-3} (9.2×10^{-4}, 1.3×10^{-3})**[b]	24.9	32.4	26.9	0.070 (0.069, 0.072)	24.9	28.9	32.4	0.63 (0.63, 0.63)
M6 + M10 + M12	n/a	n/a	402	366	425	402	449	0.12 (0.12, 0.12)	366	424	432	0.072 (0.071, 0.074)	366	424	442	0.037 (0.036, 0.038)
M7	37.7	48.9	26.9	27.9	29.6	23.3	29.6	n/a[c]	27.9	27.8	25.8	n/a[c]	27.9	31.0	24.5	n/a[c]
M8	0	14.3	20.5	19.2	20.3	18.2	24.0	0.25 (0.25, 0.25)	19.2	23.2	20.2	0.54 (0.54, 0.55)	19.2	20.2	20.6	0.65 (0.65,0.65)
M9	0	14.9	5.31	5.11	6.34	5.31	5.66	0.34 (0.33, 0.34)	5.11	5.13	6.34	0.14 (0.14, 0.15)	5.11	5.13	6.49	0.13 (0.13, 0.13)
M11	0	14.0	30.8	29.1	30.5	28.8	35.2	0.28 (0.27, 0.28)	29.1	34.7	30.3	0.47 (0.46, 0.47)	29.1	30.9	32.7	0.67 (0.67, 0.67)
M13	0	70.3	1.27	1.28	1.02	0.858	1.47	0.28 (0.28, 0.28)	1.28	1.01	1.16	0.56 (0.56, 0.57)	1.28	1.01	1.16	0.67 (0.66, 0.67)
M14	20.0	21.7	4.68	4.26	4.49	4.70	4.98	0.29 (0.29, 0.29)	4.26	4.71	4.70	0.48 (0.48, 0.48)	4.26	4.70	4.75	0.54 (0.54, 0.55)
M15	29.4	37.0	1.48	1.40	1.32	1.59	1.77	n/a[c]	1.40	1.69	1.45	n/a[c]	1.40	1.41	1.65	n/a[c]
M16	0	29.6	<0.720	<0.720	<0.720	<0.720	<0.720	0.053 (0.052, 0.055)	<0.720	<0.720	<0.720	0.083 (0.082, 0.085)	<0.720	<0.720	<0.720	0.092 (0.09, 0.094)
M17	17.9	13.5	7.29	6.62	7.22	8.80	7.36	0.17 (0.16, 0.17)	6.62	7.99	8.08	0.14 (0.14, 0.14)	6.62	6.72	8.41	0.11 (0.11,0.11)
M18	38.0	11.7	15.7	19.1	15.3	18.8	13.8	n/a[c]	19.1	15.7	15.3	n/a[c]	19.1	15.0	18.3	n/a[c]
M19	77.9	41.9	0.316	<0.276	0.341	0.604	<0.276	0.028 (0.027, 0.029)	<0.276	0.313	0.517	0.028 (0.027, 0.029)	<0.276	0.313	0.535	0.024 (0.023, 0.025)
M20	0	43.3	1.13	1.44	1.07	0.942	0.989	0.64 (0.64, 0.64)	1.44	1.13	0.929	0.50 (0.49, 0.50)	1.44	0.761	1.09	0.32 (0.32, 0.33)
M21	0	38.1	<0.310	<0.310	<0.310	<0.310	<0.310	n/a[c]	<0.310	<0.310	<0.310	n/a[c]	<0.310	<0.310	<0.310	n/a[c]
M22	2.39	31.6	<0.386	0.570	<0.386	<0.386	0.475	n/a[c]	0.570	<0.386	<0.386	n/a[c]	0.570	<0.386	<0.386	n/a[c]
M23	0	25.1	1.27	1.10	1.16	1.44	1.71	0.062 (0.061, 0.064)	1.10	1.47	1.25	0.35 (0.35, 0.35)	1.10	1.33	1.36	0.50 (0.50, 0.50)
M24 + M31 + M33	n/a	n/a	3690	3840	3460	3690	3630	0.37 (0.36, 0.37)	3840	3560	3650	0.29 (0.29, 0.29)	3840	3560	3650	0.25 (0.26, 0.26)
M25	0	15.1	15.4	16.6	12.6	22.9	12.4	0.44 (0.43, 0.44)	16.6	12.5	14.3	0.84 (0.84, 0.84)	16.6	12.3	15.8	0.42 (0.42, 0.43)
M26	5.49	18.5	1.74	1.62	1.90	1.91	1.75	0.29 (0.29, 0.29)	1.62	1.70	2.03	0.051 (0.050, 0.053)	1.62	1.89	1.80	0.21 (0.20, 0.21)
M27	n/a[d]	n/a[d]	<0.164	<0.164	<0.164	<0.164	<0.164	n/a[d]	<0.164	<0.164	<0.164	n/a[d]	<0.164	<0.164	<0.164	n/a[d]
M28 + M29	n/a	n/a	274	242	250	276	323	**0.0050 (0.0046, 0.0055)**[b]	242	303	280	0.034 (0.033, 0.035)	242	287	280	0.027 (0.026, 0.028)
M30	49.9	19.2	6.06	9.50	5.05	<3.63	<3.63	**1×10^{-5} (2.5×10^{-7}, 5.6×10^{-5})**[b]	9.50	3.63	<3.63	**0 (0, 3.7×10^{-5})**[b]	9.50	4.30	<3.63	**0 (0, 3.7×10^{-5})**[b]
M32	22.8	20.0	3.22	2.85	3.10	3.64	3.43	0.026 (0.025, 0.026)	2.85	3.42	3.34	0.054 (0.053, 0.056)	2.85	3.31	3.42	0.042 (0.040, 0.043)
M34	46.2	33.0	1.89	1.96	1.84	2.07	1.64	0.050 (0.049, 0.051)	1.96	1.67	2.07	0.099 (0.097, 0.10)	1.96	1.67	2.02	0.31 (0.31, 0.31)
M35	23.0	39.4	1.06	1.12	0.944	1.24	1.07	0.026 (0.025, 0.027)	1.12	1.04	1.05	0.81 (0.81, 0.81)	1.12	1.03	1.12	0.43 (0.43, 0.43)
M36	n/a[d]	n/a[d]	<0.453	<0.453	<0.453	<0.453	<0.453	n/a[d]	<0.453	<0.453	<0.453	n/a[d]	<0.453	<0.453	<0.453	n/a[d]
M37 + M40 + M41	n/a	n/a	317	346	283	337	302	0.10 (0.10, 0.11)	346	279	323	0.035 (0.034, 0.036)	346	273	323	0.016 (0.016, 0.017)

DOI: 10.1021/acs.est.6b03955
Environ. Sci. Technol. 2017, 51, 46−57

Table 2. continued

adduct or cluster	CV_P (%)	CV_M (%)	global median (n = 39)	medians for fuel type: control (n = 10)	smoky (n = 10)	wood (n = 9)	smokeless (n = 10)	KW P-value (95% CI)	medians for BaP exposure category: control (n = 10)	low (n = 15)	high (n = 14)	KW P-value (95% CI)	medians for $PM_{2.5}$ exposure category: control (n = 10)	low (n = 15)	high (n = 14)	KW P-value (95% CI)
M38	30.0	35.1	4.46	5.20	4.04	5.17	3.62	n/a[c]	5.20	3.91	5.02	n/a[c]	5.20	3.59	4.67	n/a[c]
M39	0	35.4	0.970	1.26	0.831	0.443	1.01	0.065 (0.063, 0.066)	1.26	0.970	0.662	0.049 (0.048, 0.050)	1.26	0.970	0.509	0.031 (0.030, 0.032)
M42	0	36.3	1.43	1.20	1.37	1.64	1.59	0.82 (0.82, 0.83)	1.20	1.51	1.48	0.74 (0.74, 0.74)	1.20	1.12	1.80	0.017 (0.016, 0.018)
M43	17.9	12.3	21.5	28.9	20.2	24.5	19.1	**5.6×10^{-4} (4.2×10^{-4}, 7.3×10^{-4})**[b]	28.9	19.1	21.1	**3.8×10^{-4} (2.7×10^{-4}, 5.2×10^{-4})**[b]	28.9	19.4	21.1	**6.2×10^{-4} (4.8×10^{-4}, 7.9×10^{-4})**[b]
M44	5.41	13.7	31.3	45.9	25.9	31.3	28.8	**1.5×10^{-4} (8.4×10^{-5}, 2.5×10^{-4})**[b]	45.9	26.3	27.1	**6.0×10^{-5} (2.2×10^{-5}, 1.3×10^{-4})**[b]	45.9	26.3	29.0	**7.0×10^{-5} (2.8×10^{-5}, 1.4×10^{-4})**[b]
M45	0	22.3	5.34	4.79	5.08	5.63	5.09	0.44 (0.43, 0.44)	4.79	5.30	5.43	0.60 (0.60, 0.60)	4.79	4.82	5.44	0.57 (0.56, 0.57)
M46	4×10^{-6}	24.6	0.783	<0.778	<0.778	0.934	0.921	0.25 (0.25, 0.25)	<0.778	0.783	0.898	0.31 (0.31, 0.32)	<0.778	<0.778	0.946	0.13 (0.13, 0.14)
M47	17.8	13.6	23.5	18.7	23.5	21.4	28.0	0.39 (0.38, 0.39)	18.7	25.4	23.4	0.35 (0.35, 0.35)	18.7	24.0	23.7	0.41 (0.41, 0.41)
M48	35.2	32.3	2.05	2.06	2.26	2.30	1.67	0.12 (0.12, 0.12)	2.06	1.74	2.36	0.012 (0.011, 0.013)	2.06	2.02	2.05	0.57 (0.57, 0.58)
M49	49.0	35.5	2.73	3.02	2.61	3.76	2.40	n/a[c]	3.02	2.73	2.65	n/a[c]	3.02	2.59	3.60	n/a[c]
M50	35.6	47.6	0.975	1.12	1.11	1.05	0.863	n/a[c]	1.12	0.875	1.39	n/a[c]	1.12	0.876	1.16	n/a[c]

[a]HK: housekeeping peptide; CV_P: coefficient of variation for replicate samples; CV_M: coefficient of variation for replicate injections; P-values and confidence interval (CI) from permuted Kruskal–Wallis (KW) tests. Left-censored (nondetect) median PARs are represented by "<" minimum (subject-specific PAR estimate). [b]Values in boldface represent significant P-values after adjustment for multiple testing using the Benjamini-Hochberg method. [c]Dropped from statistical analyses because the intraclass correlation coefficient (ICC) < 0.1. [d]Dropped from statistical analyses due to insufficient observations for fitting the mixed-effects model.

DOI: 10.1021/acs.est.6b03955
Environ. Sci. Technol. 2017, 51, 46−57

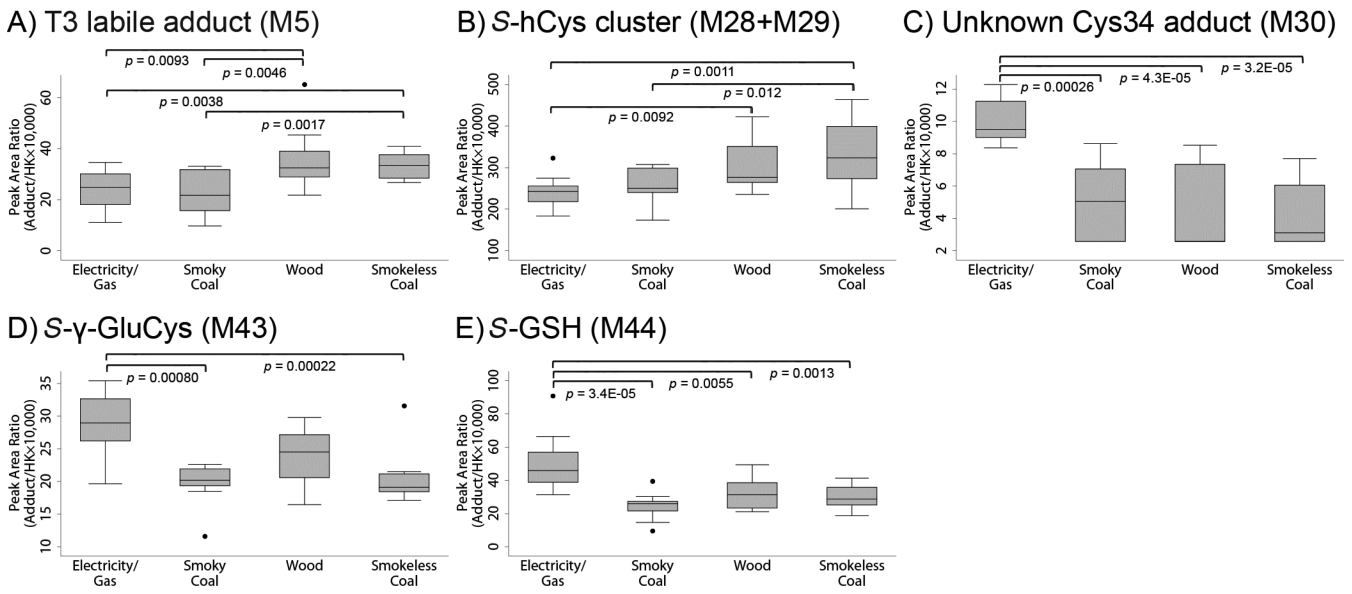

Figure 1. Pairwise comparisons of adducts showing significant global differences across fuel groups by Kruskal–Wallis tests (Table 2): (A) the labile T3 adduct (M5), (B) the *S*-hCys cluster, (C) a Cys34 adduct with unknown annotation (M30), (D) *S*-γ-GluCys (M43), and (E) *S*-GSH (M44). *P*-values indicate significant Wilcoxon rank sum tests after correction for multiple testing.

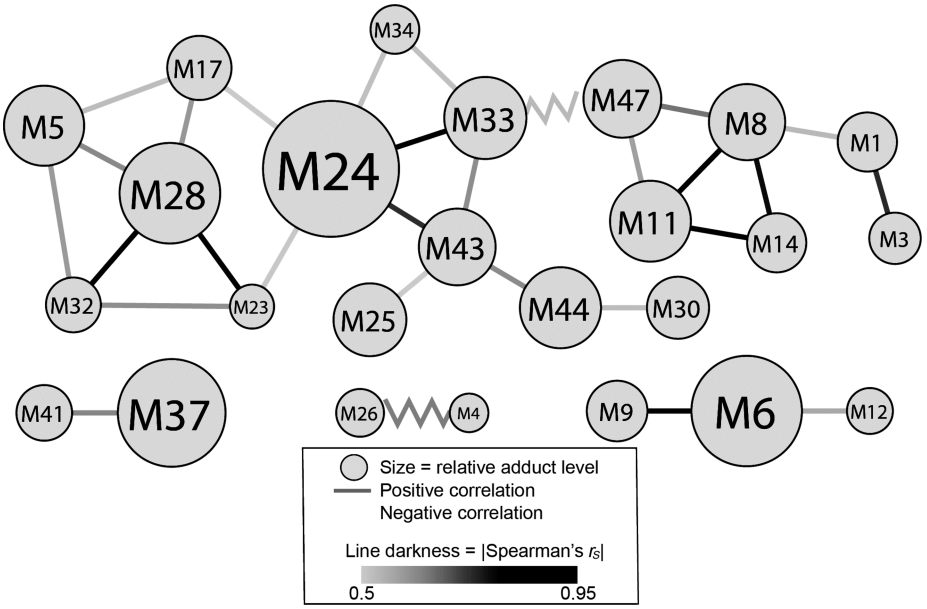

Figure 2. Map displaying adducts with moderate to very strong Spearman correlations ($|r_S| > 0.5$). Each adduct is represented by a circle, whose area is linearly related to the median logged adduct level. Each correlation is represented by a line, whose darkness corresponds to the strength of correlation.

S-Cys (M24), and *S*-CysGly (M37) were correlated with their potassium adducts (M12, M33, and M41, respectively). Oxidation products (M8, M11, and M14) were very strongly correlated with each other, as well as with Cys34 truncations (M1 and M3). In fact, the Cys34-Gln cross-link (M8) and sulfinic acid (M11) had the strongest overall correlation (r_S = 0.95). Grigoryan et al.[24] proposed two pathways of cross-link formation between Cys34 and Gln33, from the Cys34 sulfenic acid (−SOH) or from the sulfinic acid ($-SO_2H$), the latter of which is corroborated by our data.

Multivariable Models. We regressed the log-scale estimates of levels of each of the 32 adducts and clusters with sufficient data on the covariates of fuel type, ln(BaP), and age to identify significant covariate effects and reduce possible confounding (Table 3). Models for 9 adducts (M5, M17, M19, M25, M30, M32, M34, M43, and M44) contained at least one significant effect with a *P*-value <0.05 (18 in all). All of the 12 significant effects for fuel group were negative, implying that, after adjusting for BaP and age, the use of each solid fuel was typically associated with lower adduct levels than those in controls. On the other hand, all four of the significant BaP effects (M5, M19, M34, and M44) were positive, indicating that exposure to BaP increased levels of these adducts after adjusting for fuel type and age. Also, both of the significant effects of age (M17 and M32) were positive, suggesting that levels of these two adducts increased significantly with age. Only two of the 18 covariate

DOI: 10.1021/acs.est.6b03955
Environ. Sci. Technol. 2017, 51, 46–57

Table 3. Results of Multivariable Linear Regression Models with ln(Peak Area Ratio × 10 000) for Each Adduct or Cluster as the Dependent Variable[a]

adduct or cluster	intercept	smokeless	smoky	wood	ln(BaP)	age	adj. R^2 (%)
Cys34 → Gly, M1	1.7	−0.50 (0.11)	−0.68 (0.14)	−0.56 (0.27)	0.22 (0.11)	−0.0049 (0.32)	3.6
Cys34 → Oxoalanine, M3	1.2	−0.49 (0.12)	−0.76 (0.10)	−0.51 (0.31)	0.17 (0.20)	−0.0062 (0.20)	5.4
not Cys34 adduct, M4	0.45	−0.093 (0.86)	−0.15 (0.84)	−0.021 (0.98)	−0.20 (0.37)	−0.0028 (0.73)	14
T3 labile adduct, M5	2.7	−0.062 (0.81)	**−0.80 (0.043)**	−0.43 (0.31)	**0.23 (0.045)**	0.0061 (0.13)	38
unadducted T3 cluster, M6 + M10 + M12	6.0	−0.044 (0.81)	−0.26 (0.33)	−0.31 (0.29)	0.12 (0.14)	−0.0032 (0.26)	3.9
Cys34-Gln cross-link, M8	2.9	−0.10 (0.72)	−0.57 (0.19)	−0.69 (0.15)	0.21 (0.099)	−0.0031 (0.50)	5.6
methylation, not Cys34, M9	1.7	−0.26 (0.36)	−0.60 (0.16)	−0.72 (0.12)	0.23 (0.062)	−0.0037 (0.41)	2.4
sulfinic acid, M11	3.4	−0.095 (0.72)	−0.49 (0.22)	−0.53 (0.22)	0.17 (0.15)	−0.0022 (0.60)	0.073
S-methylthiolation, M13	0.13	−0.26 (0.59)	−0.71 (0.32)	−0.96 (0.23)	0.17 (0.43)	0.00027 (0.97)	0
sulfonic acid, M14	1.4	0.070 (0.56)	−0.032 (0.86)	−0.067 (0.73)	0.022 (0.67)	0.00076 (0.69)	0
pyruvate or malonate semialdehyde, M16	1.8	−0.91 (0.32)	−1.6 (0.24)	−1.4 (0.35)	0.061 (0.88)	−0.021 (0.15)	17
S-mercaptoacetic acid, M17	1.4	−0.090 (0.70)	−0.18 (0.61)	−0.12 (0.75)	0.091 (0.36)	**0.0074 (0.049)**	11
S-Cys (possibly NH_2 → OH, $-H_2O$), M19	−1.6	**−0.76 (0.045)**	−1.0 (0.071)	−0.68 (0.27)	**0.38 (0.022)**	0.0028 (0.64)	30
benzaldehyde, M20	−0.24	0.30 (0.75)	1.6 (0.26)	1.3 (0.41)	−0.50 (0.23)	0.020 (0.19)	0
S-hCys ($-H_2O$), M23	−0.25	0.050 (0.89)	−0.71 (0.21)	−0.55 (0.37)	0.20 (0.22)	0.0046 (0.44)	12
S-Cys cluster, M24 + M31 + M33	8.2	−0.19 (0.074)	−0.24 (0.12)	−0.22 (0.20)	0.041 (0.35)	0.0019 (0.25)	4.2
S-Cys (NH_2 → OH), M25	2.3	−0.58 (0.099)	**−1.1 (0.042)**	−0.92 (0.11)	0.26 (0.085)	0.0060 (0.27)	5.2
Cys34 adduct with unknown annotation, M26	0.37	−0.16 (0.45)	−0.29 (0.34)	−0.26 (0.44)	0.13 (0.14)	−0.000041 (0.99)	2.3
S-hCys cluster, M28 + M29	5.2	0.059 (0.70)	−0.29 (0.20)	−0.20 (0.41)	0.11 (0.11)	0.0048 (0.051)	33
Cys34 adduct with unknown annotation, M30	2.7	**−0.80 (0.036)**	−0.63 (0.26)	−0.75 (0.22)	−0.044 (0.78)	−0.0069 (0.24)	42
S-hCys, plus methylation not at Cys34, M32	0.67	0.052 (0.78)	−0.32 (0.24)	−0.24 (0.43)	0.12 (0.13)	**0.0059 (0.045)**	29
S-CysGly ($-H_2O$), M34	0.72	**−0.41 (0.010)**	**−0.50 (0.033)**	−0.33 (0.19)	**0.13 (0.050)**	−0.0025 (0.31)	25
S-(*N*-Acetyl)Cys, M35	−0.10	−0.25 (0.34)	−0.62 (0.12)	−0.34 (0.44)	0.14 (0.24)	0.0016 (0.70)	5.5
S-CysGly cluster, M37 + M40 + M41	6.0	−0.16 (0.35)	−0.20 (0.44)	−0.068 (0.81)	−0.00075 (0.99)	−0.0028 (0.31)	5.2
Cys34 adduct with unknown annotation, M39	1.1	−0.14 (0.81)	−0.070 (0.94)	−0.29 (0.76)	−0.19 (0.45)	−0.0097 (0.30)	17
Cys34 adduct with unknown annotation, M42	−0.50	−0.035 (0.95)	0.21 (0.79)	0.35 (0.69)	−0.096 (0.67)	0.015 (0.073)	0
S-γ-GluCys, M43	3.2	**−0.52 (0.00 −16)**	**−0.66 (0.0066)**	**−0.51 (0.048)**	0.087 (0.20)	0.0017 (0.49)	38
S-GSH, M44	3.9	**−0.91 (0.0010)**	**−1.5 (0.00056)**	**−1.2 (0.0070)**	**0.22 (0.049)**	−0.0033 (0.41)	44
Cys34 adduct with unknown annotation, M45	1.9	0.13 (0.62)	0.15 (0.70)	0.39 (0.37)	−0.037 (0.75)	−0.0067 (0.12)	0
unclear modification site, M46	−0.80	0.11 (0.70)	−0.11 (0.78)	−0.010 (0.98)	0.049 (0.68)	0.0075 (0.090)	6.4
Cys34 adduct with unknown annotation, M47	3.0	0.36 (0.31)	0.29 (0.58)	0.20 (0.73)	−0.033 (0.83)	−0.00069 (0.90)	0
Cys34 adduct with unknown annotation, M48	0.61	−0.21 (0.38)	−0.032 (0.93)	0.14 (0.72)	−0.017 (0.87)	0.0022 (0.57)	5.2

[a]Each row shows the modeled adduct (or cluster) and regression coefficients (with *P*-values in parentheses) for each covariate. (The three fuel types, i.e., smoky and smokeless coal and wood, were dichotomous variables with electricity/gas as the reference group, and ln(BaP) (ng/m^3) and age were continuous variables). Values in boldface represent *P*-values <0.05.

effects with *P*-values <0.05 were significant after FDR adjustment (α = 0.0017), namely, *S*-GSH (M44) and *S*-γ-GluCys (M43), consistent with the univariate analyses. Interestingly, the *S*-hCys cluster (M28 and M29), which had been strongly associated with fuel type in univariate analyses (Table 2 and Figure 1B), did not detect the same associations after adjustment for BaP and age, both of which were marginally associated with *S*-hCys levels (Table 3). Also, the strong effects of fuel type and BaP on levels of the unannotated adduct, M30 (Table 2), were greatly reduced in the multivariable model, where only smokeless coal showed evidence of an association (*P*-value = 0.036).

DISCUSSION

This is the first application of Cys34 adductomics to investigate populations exposed to high levels of combustion products that are known to contribute to lung disease. Indeed, nonsmoking women exposed to indoor emissions from smoky coal have among the highest lung cancer incidence and mortality in the world.[5,6] Constituents of smoky coal and its emissions have been explored in an attempt to pinpoint those that account for lung cancer risk.[7−10,25,26] Here, we integrated untargeted adductomics with external exposure measurements to investigate the influence of fuel type and external exposures on downstream biological processes that are reflected by Cys34 adducts.

The 50 T3-peptides detected in this study of Chinese women are similar to the 43 T3-peptides reported by Grigoryan et al.,[23] who applied the same methodology to plasma from healthy smokers and nonsmokers in the U.S. The Venn diagram in Figure S3 compares the features reported from these two studies, 31 of which were detected in both. Grigoryan et al.[23] reported that

DOI: 10.1021/acs.est.6b03955
Environ. Sci. Technol. 2017, 51, 46−57

cigarette smokers had significantly higher levels of adducts representing Cys34 addition of ethylene oxide and acrylonitrile (two constituents of cigarette smoke) as well as the T3-methylation product and also had decreased levels of the Cys34 sulfinic acid and Cys34-*S*-Cys adduct. All of the women in the current study were nonsmokers, and a different set of adducts was identified that distinguished solid fuel users from controls.

The most prominent class of Cys34 adducts detected in our investigation were the Cys34 mixed disulfides (22 of 50 T3 features in Table 1) that reflect reactions with low-molecular-weight thiols.[35] The median contributions of the five most abundant Cys34 disulfides are compared in Table S3 with those from targeted analysis of the same species in another investigation by Lepedda et al.[36] The similar percentages derived from sets of independent data indicate that our Cys34 adductomics pipeline is quantitatively reliable.

Several adducts detected in our study were significantly associated with the fuel type and BaP exposures. The strongest associations between adduct levels and fuel type involved the disulfides *S*-GSH (M44) and *S*-γ-GluCys (M43) (Tables 2 and 3). Intracellular GSH plays a principle role in the elimination of reactive electrophiles, including ROS, and is depleted under oxidative stress.[37,38] The *S*-GSH adduct represents the reaction between Cys34 and GSH that can involve the unstable Cys34 sulfenic acid (−SOH) as an intermediate.[20] Thus, the lower levels of *S*-GSH observed in the solid fuel groups relative to controls could reflect depletion of intracellular GSH that is mediated by exposures to reactive electrophiles generated by combustion products from solid fuels.

Using the estimated regression coefficients from multivariable models (Table 3), the fold change (control: exposed) for smoky coal = 1/exp(−1.4522) = 4.27 compared to 3.30 for wood and 2.49 for smokeless coal. This indicates that the *S*-GSH adduct was present at lower concentrations in smoky-coal users compared to smokeless-coal and wood-fuel users after adjustment for BaP exposure and age and suggests that smoky coal may be a more potent cause of GSH depletion than either smokeless coal or wood.

Decreased levels of circulating GSH have been observed in various diseases and cancers,[35] and the null genotype of glutathione *S*-transferase M1 was associated with increased lung-cancer risk in Asian populations exposed to indoor combustion of coal[39] and smoky coal in Xuanwei County.[13] Similar decreases in the *S*-γ-GluCys adduct (Table 3) probably reflect the fact that γ-GluCys is a dipeptide precursor for the GSH tripeptide.[40] Membrane-bound γ-glutamyltranspeptidase catabolizes conversion of extracellular GSH to CysGly, stimulating the production of pro-oxidant species, and is upregulated in various cancer cells and by depletion of intracellular GSH.[38,40−42] It is interesting that the ratio of Cys34-*S*-CysGly (M34) to Cys34-*S*-GSH (M44) was elevated in all exposed groups relative to controls (Figure 3), especially for smoky coal which showed a much stronger effect (*P*-value = 0.00042) than for wood-fuel (*P*-value = 0.031) or smokeless coal (*P*-value = 0.034). This suggests that γ-glutamyltranspeptidase activity may have contributed to the decrease in circulating GSH via catabolism to CysGly, especially for subjects using smoky coal.

One adduct that differed substantially across fuel types was the T3 labile adduct (M5) which has been reported previously.[23] We suspect that this labile adduct disaggregates in the nanoelectrospray source because it has an accurate mass and MS2 spectrum identical to those of the unadducted T3 peptide

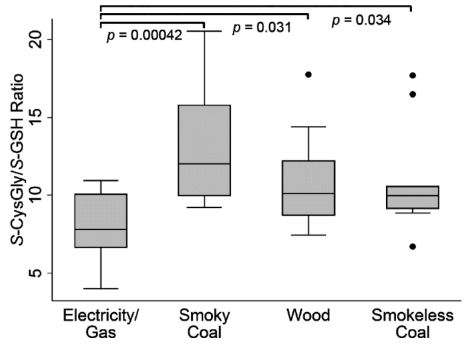

Figure 3. Pairwise comparisons of ratios of *S*-CysGly (M37 + M40 + M41) to *S*-GSH (M44) across fuel groups (Kruskal−Wallis, *P*-value = 0.0107).

but has a distinct retention time (eluting about 30 s earlier than the T3 peptide). Levels of this labile adduct were significantly lower in users of smoky coal compared to other fuel groups after adjustment for exposure to BaP and age but increased with exposure to BaP after adjusting for fuel type and age (Table 3). Although the identity of this adduct has not been ascertained, its levels were correlated with several Cys34 disulfides, particularly M17 (*S*-mercaptoacetic acid) and the two isoforms of *S*-hCys (M28 and M32). However, in our previous adductomic analysis, we observed that this labile T3 adduct was not affected by TCEP treatment, suggesting that it is not a Cys34 disulfide.[23]

Further research is required to annotate a number of adducts that were associated with exposure to combustion products, particularly the labile T3 adduct (M5) and M30 (likely composition, $+C_4H_9O_3S$). Also, the relationship between levels of *S*-hCys (M28 + M29) and solid fuel, which was highly significant in univariate analyses (Table 2) but not in the multivariable model (Table 3), requires additional investigation.

In summary, our study detected a host of HSA adducts in plasma from 39 nonsmoking Chinese women. Several of these adducts were significantly influenced by solid fuel use and pollutant exposures, particularly *S*-GSH and *S*-γ-GluCys, which were both present at lower levels in subjects using solid fuels than in controls (Tables 2 and 3). We realize that this study is small and will require validation with larger samples sizes. Another limitation is the lack of measurements of $PM_{2.5}$ and BaP exposures among control subjects, although it is reasonable to expect that nonsmoking controls who used electricity/gas had lower exposures to $PM_{2.5}$ and BaP than the solid fuel users.

■ ASSOCIATED CONTENT

Supporting Information

The Supporting Information is available free of charge on the ACS Publications website at DOI: 10.1021/acs.est.6b03955.

MS2 spectra of putative T3 peptides; pairwise comparisons of adducts showing significant global differences across exposure categories; Venn diagram comparing common and unique adducts with those reported by Grigoryan et al.;[23] summary statistics of subjects' characteristics (mean ± SD) across fuel types; evidence used to annotate putative T3 adducts; relative percentages of 5 plasma HSA-Cys34 mixed disulfides detected in the current study and in an independent study by Lepedda et al.[36] (PDF)

■ AUTHOR INFORMATION

Corresponding Author

*Tel.:510 642-4355; e-mail: srappaport@berkeley.edu.

DOI: 10.1021/acs.est.6b03955
Environ. Sci. Technol. 2017, 51, 46−57

ORCID

Sixin S. Lu: 0000-0001-9951-1721

Stephen M. Rappaport: 0000-0002-3806-0848

Author Contributions

[▽]H.G., Q.L., and S.M.R. cosupervised this work.

Notes

The authors declare no competing financial interest.

■ ACKNOWLEDGMENTS

This work was supported by Grant R33CA191159 and by the intramural program of the National Cancer Institute of the U.S. National Institutes of Health. The authors also acknowledge support from Grants U54ES016115 and R44ES022360 from the National Institute for Environmental Health Sciences. The content is solely the responsibility of the authors and does not necessarily represent the official views of the National Institutes of Health.

■ ABBREVIATIONS

BaP	benzo(*a*)pyrene
CV	coefficient of variation
CysGly	cysteinylglycine
FDR	false discovery rate
γ-GluCys	γ-glutamylcysteine
GSH	glutathione
hCys	homocysteine
HK	"housekeeping peptide"
HRMS	high-resolution mass spectrometry
HSA	human serum albumin
IAA-iT3	carbamidomethylated iT3 peptide internal standard
ICC	intraclass correlation
iT3	isotopically labeled T3 peptide
MIM	monoisotopic mass
nLC	nanoflow liquid chromatography
PAH	polycyclic aromatic hydrocarbon
PM	particulate matter
$PM_{2.5}$	particulate matter with aerodynamic diameter less than 2.5 μm
r_S	Spearman correlation coefficient
ROS	reactive oxygen species
RT	retention time
T3	third largest peptide after tryptic digestion of HSA which includes Cys34

■ REFERENCES

(1) Torre, L. A.; Bray, F.; Siegel, R. L.; Ferlay, J.; Lortet-Tieulent, J.; Jemal, A. Global cancer statistics, 2012. *Ca-Cancer J. Clin.* **2015**, *65* (2), 87−108.

(2) Sun, S.; Schiller, J. H.; Gazdar, A. F. Lung cancer in never smokers–a different disease. *Nat. Rev. Cancer* **2007**, *7* (10), 778−90.

(3) Hosgood, H. D., 3rd; Boffetta, P.; Greenland, S.; Lee, Y. C.; McLaughlin, J.; Seow, A.; Duell, E. J.; Andrew, A. S.; Zaridze, D.; Szeszenia-Dabrowska, N.; Rudnai, P.; Lissowska, J.; Fabianova, E.; Mates, D.; Bencko, V.; Foretova, L.; Janout, V.; Morgenstern, H.; Rothman, N.; Hung, R. J.; Brennan, P.; Lan, Q. In-home coal and wood use and lung cancer risk: a pooled analysis of the International Lung Cancer Consortium. *Environ. Health Perspect.* **2010**, *118* (12), 1743−7.

(4) Smith, K. R.; Bruce, N.; Balakrishnan, K.; Adair-Rohani, H.; Balmes, J.; Chafe, Z.; Dherani, M.; Hosgood, H. D.; Mehta, S.; Pope, D.; Rehfuess, E.; et al. Millions dead: how do we know and what does it mean? Methods used in the comparative risk assessment of household air pollution. *Annu. Rev. Public Health* **2014**, *35*, 185−206.

(5) Barone-Adesi, F.; Chapman, R. S.; Silverman, D. T.; He, X.; Hu, W.; Vermeulen, R.; Ning, B.; Fraumeni, J. F., Jr.; Rothman, N.; Lan, Q. Risk of lung cancer associated with domestic use of coal in Xuanwei, China: retrospective cohort study. *Bmj* **2012**, *345*, e5414.

(6) Mumford, J. L.; He, X. Z.; Chapman, R. S.; Cao, S. R.; Harris, D. B.; Li, X. M.; Xian, Y. L.; Jiang, W. Z.; Xu, C. W.; Chuang, J. C.; Wilson, W. E.; Cooke, M. Lung-Cancer and Indoor Air-Pollution in Xuan-Wei, China. *Science* **1987**, *235* (4785), 217−220.

(7) Lan, Q.; He, X.; Shen, M.; Tian, L.; Liu, L. Z.; Lai, H.; Chen, W.; Berndt, S. I.; Hosgood, H. D.; Lee, K. M.; Zheng, T.; Blair, A.; Chapman, R. S. Variation in lung cancer risk by smoky coal subtype in Xuanwei, China. *Int. J. Cancer* **2008**, *123* (9), 2164−9.

(8) Hu, W.; Downward, G. S.; Reiss, B.; Xu, J.; Bassig, B. A.; Hosgood, H. D., 3rd; Zhang, L.; Seow, W. J.; Wu, G.; Chapman, R. S.; Tian, L.; Wei, F.; Vermeulen, R.; Lan, Q. Personal and indoor PM2.5 exposure from burning solid fuels in vented and unvented stoves in a rural region of China with a high incidence of lung cancer. *Environ. Sci. Technol.* **2014**, *48* (15), 8456−64.

(9) Downward, G. S.; Hu, W.; Rothman, N.; Reiss, B.; Wu, G.; Wei, F.; Chapman, R. S.; Portengen, L.; Qing, L.; Vermeulen, R. Polycyclic aromatic hydrocarbon exposure in household air pollution from solid fuel combustion among the female population of Xuanwei and Fuyuan counties, China. *Environ. Sci. Technol.* **2014**, *48* (24), 14632−41.

(10) Downward, G. S.; Hu, W.; Large, D.; Veld, H.; Xu, J.; Reiss, B.; Wu, G.; Wei, F.; Chapman, R. S.; Rothman, N.; Qing, L.; Vermeulen, R. Heterogeneity in coal composition and implications for lung cancer risk in Xuanwei and Fuyuan counties, China. *Environ. Int.* **2014**, *68*, 94−104.

(11) Mumford, J. L.; Lee, X.; Lewtas, J.; Young, T. L.; Santella, R. M. DNA adducts as biomarkers for assessing exposure to polycyclic aromatic hydrocarbons in tissues from Xuan Wei women with high exposure to coal combustion emissions and high lung cancer mortality. *Environ. Health Perspect* **1993**, *99*, 83−7.

(12) Hosgood, H. D., 3rd; Pao, W.; Rothman, N.; Hu, W.; Pan, Y. H.; Kuchinsky, K.; Jones, K. D.; Xu, J.; Vermeulen, R.; Simko, J.; Lan, Q. Driver mutations among never smoking female lung cancer tissues in China identify unique EGFR and KRAS mutation pattern associated with household coal burning. *Respiratory medicine* **2013**, *107* (11), 1755−62.

(13) Lan, Q.; He, X.; Costa, D. J.; Tian, L.; Rothman, N.; Hu, G.; Mumford, J. L. Indoor coal combustion emissions, GSTM1 and GSTT1 genotypes, and lung cancer risk: a case-control study in Xuan Wei, China. *Cancer Epidemiol Biomarkers Prev* **2000**, *9* (6), 605−608.

(14) Lan, Q.; Mumford, J. L.; Shen, M.; Demarini, D. M.; Bonner, M. R.; He, X.; Yeager, M.; Welch, R.; Chanock, S.; Tian, L.; Chapman, R. S.; Zheng, T.; Keohavong, P.; Caporaso, N.; Rothman, N. Oxidative damage-related genes AKR1C3 and OGG1 modulate risks for lung cancer due to exposure to PAH-rich coal combustion emissions. *Carcinogenesis* **2004**, *25* (11), 2177−2181.

(15) Miller, E. C.; Miller, J. A. Mechanisms of chemical carcinogenesis: nature of proximate carcinogens and interactions with macromolecules. *Pharmacol Rev.* **1966**, *18* (1), 805−838.

(16) Brodie, B. B.; Reid, W. D.; Cho, A. K.; Sipes, G.; Krishna, G.; Gillette, J. R. Possible mechanism of liver necrosis caused by aromatic organic compounds. *Proc. Natl. Acad. Sci. U. S. A.* **1971**, *68* (1), 160−4.

(17) Go, Y. M.; Jones, D. P. The redox proteome. *J. Biol. Chem.* **2013**, *288* (37), 26512−20.

(18) Rubino, F. M.; Pitton, M.; Di Fabio, D.; Colombi, A. Toward an "omic" physiopathology of reactive chemicals: thirty years of mass spectrometric study of the protein adducts with endogenous and xenobiotic compounds. *Mass Spectrom. Rev.* **2009**, *28* (5), 725−84.

(19) Aldini, G.; Vistoli, G.; Regazzoni, L.; Gamberoni, L.; Facino, R. M.; Yamaguchi, S.; Uchida, K.; Carini, M. Albumin is the main nucleophilic target of human plasma: a protective role against pro-atherogenic electrophilic reactive carbonyl species? *Chem. Res. Toxicol.* **2008**, *21* (4), 824−35.

(20) Carballal, S.; Alvarez, B.; Turell, L.; Botti, H.; Freeman, B. A.; Radi, R. Sulfenic acid in human serum albumin. *Amino Acids* **2007**, *32* (4), 543−51.

DOI: 10.1021/acs.est.6b03955
Environ. Sci. Technol. 2017, 51, 46−57

(21) Aldini, G.; Yeum, K.-J.; Vistoli, G. Covalent Modifications of Albumin Cys34 as a Biomarker of Mild Oxidative Stress. In *Biomarkers for Antioxidant Defense and Oxidative Damage: Principles and Practical Applications*; Aldini, G., Yeum, K.-J., Niki, E., Russell, R. M., Eds. Wiley-Blackwell: Hoboken, NJ, 2010; pp 229−241.
(22) Nagumo, K.; Tanaka, M.; Chuang, V. T.; Setoyama, H.; Watanabe, H.; Yamada, N.; Kubota, K.; Tanaka, M.; Matsushita, K.; Yoshida, A.; Jinnouchi, H.; Anraku, M.; Kadowaki, D.; Ishima, Y.; Sasaki, Y.; Otagiri, M.; Maruyama, T. Cys34-cysteinylated human serum albumin is a sensitive plasma marker in oxidative stress-related chronic diseases. *PLoS One* **2014**, *9* (1), e85216.
(23) Grigoryan, H.; Edmands, W.; Lu, S. S.; Yano, Y.; Regazzoni, L.; Iavarone, A. T.; Williams, E. R.; Rappaport, S. M. Adductomics Pipeline for Untargeted Analysis of Modifications to Cys34 of Human Serum Albumin. *Anal. Chem.* **2016**, *88* (21), 10504−10512.
(24) Grigoryan, H.; Li, H.; Iavarone, A. T.; Williams, E. R.; Rappaport, S. M. Cys34 adducts of reactive oxygen species in human serum albumin. *Chem. Res. Toxicol.* **2012**, *25* (8), 1633−42.
(25) Hosgood, H. D.; Vermeulen, R.; Wei, H.; Reiss, B.; Coble, J.; Wei, F.; Jun, X.; Wu, G.; Rothman, N.; Lan, Q. Combustion-derived nanoparticle exposure and household solid fuel use in Xuanwei and Fuyuan, China. *Int. J. Environ. Health Res.* **2012**, *22* (6), 571−81.
(26) Seow, W. J.; Hu, W.; Vermeulen, R.; Hosgood Iii, H. D.; Downward, G. S.; Chapman, R. S.; He, X.; Bassig, B. A.; Kim, C.; Wen, C.; Rothman, N.; Lan, Q. Household air pollution and lung cancer in China: a review of studies in Xuanwei. *Chin. J. Cancer* **2014**, *33* (10), 471−475.
(27) Chambers, M. C.; Maclean, B.; Burke, R.; Amodei, D.; Ruderman, D. L.; Neumann, S.; Gatto, L.; Fischer, B.; Pratt, B.; Egertson, J.; Hoff, K.; Kessner, D.; Tasman, N.; Shulman, N.; Frewen, B.; Baker, T. A.; Brusniak, M. Y.; Paulse, C.; Creasy, D.; Flashner, L.; Kani, K.; Moulding, C.; Seymour, S. L.; Nuwaysir, L. M.; Lefebvre, B.; Kuhlmann, F.; Roark, J.; Rainer, P.; Detlev, S.; Hemenway, T.; Huhmer, A.; Langridge, J.; Connolly, B.; Chadick, T.; Holly, K.; Eckels, J.; Deutsch, E. W.; Moritz, R. L.; Katz, J. E.; Agus, D. B.; MacCoss, M.; Tabb, D. L.; Mallick, P. A cross-platform toolkit for mass spectrometry and proteomics. *Nat. Biotechnol.* **2012**, *30* (10), 918−20.
(28) The R Foundation. *R: A language and environment for statistical computing*; R Foundation for Statistical Computing: Vienna, Austria, 2014.
(29) Patiny, L.; Borel, A. ChemCalc: a building block for tomorrow's chemical infrastructure. *J. Chem. Inf. Model.* **2013**, *53* (5), 1223−8.
(30) Wolf, S.; Schmidt, S.; Muller-Hannemann, M.; Neumann, S. In silico fragmentation for computer assisted identification of metabolite mass spectra. *BMC Bioinf.* **2010**, *11*, 148.
(31) Benjamini, Y.; Hochberg, Y. Controlling the False Discovery Rate: a Practical and Powerful Approach to Multiple Testing. *Journal of the Royal Statistical Society* **1995**, *57* (1), 289−300.
(32) Newson, R. *SMILEPLOT: Stata module to create plots for use with multiple significance tests*; Statistical Software Components, Boston College: Chestnut Hill, MA, 2012.
(33) Dinno, A. *dunn-test: Dunn's Test of Multiple Comparisons Using Rank Sums*; 2014; http://www.alexisdinno.com/stata/dunntest.html.
(34) Shannon, P.; Markiel, A.; Ozier, O.; Baliga, N. S.; Wang, J. T.; Ramage, D.; Amin, N.; Schwikowski, B.; Ideker, T. Cytoscape: a software environment for integrated models of biomolecular interaction networks. *Genome Res.* **2003**, *13* (11), 2498−2504.
(35) Isokawa, M.; Kanamori, T.; Funatsu, T.; Tsunoda, M. Analytical methods involving separation techniques for determination of low-molecular-weight biothiols in human plasma and blood. *J. Chromatogr. B: Anal. Technol. Biomed. Life Sci.* **2014**, *964*, 103−15.
(36) Lepedda, A. J.; Zinellu, A.; Nieddu, G.; De Muro, P.; Carru, C.; Spirito, R.; Guarino, A.; Piredda, F.; Formato, M. Human serum albumin Cys34 oxidative modifications following infiltration in the carotid atherosclerotic plaque. *Oxid. Med. Cell. Longevity* **2014**, *2014*, 690953.
(37) Nel, A. Atmosphere. Air pollution-related illness: effects of particles. *Science* **2005**, *308* (5723), 804−6.
(38) Pompella, A.; Visvikis, A.; Paolicchi, A.; De Tata, V.; Casini, A. F. The changing faces of glutathione, a cellular protagonist. *Biochem. Pharmacol.* **2003**, *66* (8), 1499−1503.
(39) Hosgood, H. D., III; Berndt, S. I.; Lan, Q. GST genotypes and lung cancer susceptibility in Asian populations with indoor air pollution exposures: A meta-analysis. *Mutat. Res., Rev. Mutat. Res.* **2007**, *636* (1−3), 134−143.
(40) Lu, S. C. Glutathione synthesis. *Biochim. Biophys. Acta, Gen. Subj.* **2013**, *1830* (5), 3143−53.
(41) Pompella, A.; De Tata, V.; Paolicchi, A.; Zunino, F. Expression of gamma-glutamyltransferase in cancer cells and its significance in drug resistance. *Biochem. Pharmacol.* **2006**, *71* (3), 231−8.
(42) Dominici, S.; Paolicchi, A.; Lorenzini, E.; Maellaro, E.; Comporti, M.; Pieri, L.; Minotti, G.; Pompella, A. Gamma-glutamyltransferase-dependent prooxidant reactions: a factor in multiple processes. *BioFactors* **2003**, *17* (1−4), 187−98.

DOI: 10.1021/acs.est.6b03955
Environ. Sci. Technol. 2017, 51, 46−57